JAERI-M
94-055

A CONCEPT OF A NEW UNDULATOR THAT WILL GENERATE IRRATIONAL HIGHER HARMONICS IN SYNCHROTRON RADIATION

March 1994

Shinya HASHIMOTO* and Shigemi SASAKI

日本原子力研究所
Japan Atomic Energy Research Institute

JAERI-Mレポートは，日本原子力研究所が不定期に公刊している研究報告書です。
入手の問合わせは，日本原子力研究所技術情報部情報資料課（〒319-11茨城県那珂郡東海村）あて，お申しこしください。なお，このほかに財団法人原子力弘済会資料センター（〒319-11 茨城県那珂郡東海村日本原子力研究所内）で複写による実費頒布をおこなっております。

JAERI-M reports are issued irregularly.
Inquiries about availability of the reports should be addressed to Information Division Department of Technical Information, Japan Atomic Energy Research Institute, Tokai-mura, Naka-gun, Ibaraki-ken 319-11, Japan.

編集兼発行　日本原子力研究所
印　　刷　いばらき印刷㈱

JAERI-M 94-055

A Concept of a New Undulator That will Generate Irrational Higher Harmonics in Synchrotron Radiation

Shinya HASHIMOTO* and Shigemi SASAKI

Department of Synchrotron Radiation Facility Project
Tokai Research Establishment
Japan Atomic Energy Research Institute
Tokai-mura, Naka-gun, Ibaraki-ken

(Received February 17, 1994)

A preliminary consideration has been made on an undulator with magnetic poles quasi-periodically aligned along the path of electron beams to discriminate the rational higher harmonics of radiation that are harmful in some synchrotron radiation experiments. The harmonics with irrational ratios in energy generated by the undulator is never simultaneously reflected by a crystal monochromator in the same orientation. A combination of the new undulator and high-resolution crystal monochromator is expected to be very useful on beamlines of high energy radiation in which X-ray mirrors are useless because of too small critical angles of total reflection. Further, a possibility of manufacturing the new undulator has been discussed.

Keywords: Synchrotron Radiation, Undulator, Higher Harmonics, Quasi-periodicity, Irrational Number

---

* On leave from Japan Synchrotron Radiation Research Institute

JAERI-M 94-055

放射光の無理数次高調波を発生する新しいアンジュレータの概念

日本原子力研究所大型放射光施設開設室
橋本　眞也* ・佐々木茂美

（1994年２月17日受理）

幾つかの放射光実験において害となる分数比をもつ高調波を除去するために磁極を準周期的に並べたアンジュレータについて基礎的な考察をした。このアンジュレータが発生するエネルギー比が無理数である高調波は結晶モノクロメータによって同時に反射されることはない。この種のアンジュレータは，分解能の高い結晶モノクロメータを組合わせることによって，全反射ミラーが使えない高エネルギービームラインにおいて，非常に有用となることが期待される。さらに，新しい概念を持つこのアンジュレータの実機製作の可能性についても議論している。

日本原子力研究所：〒319-11　茨城県那珂郡東海村白方白根２－４
＊高輝度光科学研究センターから出向

Contents

目　　次

Glossary

x, y	Positional variables in 2D real space.
x_i, y_i	Positional variables for the lattice point in real space.
a	Nearest neighbor distance in the 2D real lattice. This is the lattice constant of the primitive square lattice.
a'	Lattice constant of the composite lattice with two kinds of matters defined in Fig. 6. $a'=a\sqrt{2}$.
$R^{//}, R^{\perp}$	Positional variables in a coordinate system rotated by a from the xy system.
$R_i^{//}, R_i^{\perp}$	Positional variables for the lattice point corresponding to (x_i, y_i).
α	Angle of the inclination of the R// axis from the x axis.
τ	A typical irrational number for creating a quasi-periodic lattice, which is known as the golden mean taking a value of $(1+\sqrt{5})/2$.
w	Width of the window defined in real space, the lattice points in which are projected onto the R// axis.
w'	$2w$. Width of the window doubled in real space.
d, d'	Distances realized in a quasi-periodic array of matters on the R// axis.
$S(\mathbf{R})$	Structure function revealing the 2D lattice.
$V(\mathbf{R})$	Window function defined in eq. (13).
$E(\mathbf{R})$	Structure function of the lattice in the window.
$P(R^{//})$	Structure of $E(\mathbf{R})$ projected on the R// axis.
$S(\mathbf{q})$	Structure amplitude from the 2D lattice.
$V(\mathbf{q})$	Fourier transform of the window function.
h, k	Positional variables in 2D reciprocal space.
h_i, k_i	Positional variables for the reciprocal lattice point.
$q^{//}, q^{\perp}$	Positional variables in a coordinate system rotated by a from the hk system.
$q_i^{//}, q_i^{\perp}$	Positional variables of the reciprocal lattice point represented in the $(q^{//}, q^{\perp})$ system.

1. Introduction

Conventional sources for synchrotron radiation generate X-ray photons with a wide band of energy or with strong higher harmonics.[1-4] Silicon crystal is properly used for monochromating the radiation, which simultaneously reflects some higher harmonics through the same lattice planes. The higher harmonics of radiation are generally harmful in experiments and are usually removed by use of total reflection mirrors characterized by a critical angle depending on the radiation energy and atomic weight of mirror-materials. In some cases, we detune a double crystal monochromator to eliminate the higher harmonics by taking advantage of narrower Darwin curves for the higher order reflections. In the third generation facilities of synchrotron radiation, the accelerating voltage of electrons is raised up to 6-8 GeV and very high photon energies will be actively used. The conventional ways to get rid of the higher harmonics must be unsuitable or useless in such high energy usages, because of a very small critical angle of total reflection and a very narrow angular width of the Darwin curve even of the first harmonic.

For the same purpose as we described above, recently, an undulator to suppress the higer harmonics by adding a horizontal magnetic field has been reported.[5] From a completely different viewpoint, we here propose an undulator never generating rational higher harmonics but irrational ones that are never diffracted in the same orientation of monochromator crystals. Our idea originates in the diffraction property of the quasi-periodic lattices.[6-8] We know the analogy between the following two equations:

1)X-ray intensity from a one-dimensional scatterer with electron density of $\rho(r)$;

$$I(q) = \left| \int_{-\infty}^{\infty} \rho(r) \exp(2\pi i q r)\, \mathrm{d}r \right|^2 . \qquad (1)$$

2)Spectral-angular intensity distribution from undulators;[9]

$$\frac{\mathrm{d}^2 I}{\mathrm{d}f\, \mathrm{d}\Omega} = \left| \int_{-\infty}^{\infty} s(t) \exp(2\pi i f t)\, \mathrm{d}t \right|^2 , \qquad (2a)$$

$$s(t) = \left(\frac{[\mathbf{n} \times (\mathbf{n} - \dot{\mathbf{r}}/c) \times \dot{\mathbf{r}}/c\,]}{(1 - \mathbf{n} \cdot \dot{\mathbf{r}}/c)^2} \right) \exp(-2\pi i f\, \mathbf{n}.\mathbf{r}/c) \quad . \qquad (2b)$$

Time, t, in eq. (2b) is usually known as "the retarded time" or "the emitter time". Replacing dt by $(1/\mathbf{n}.\dot{\mathbf{r}})d(\mathbf{n}.\mathbf{r})$ and $s(t)$ by $s(\mathbf{n}.\mathbf{r})$, we can express the equation as a function of a distance along the lining direction of magnets, $(\mathbf{n}.\mathbf{r})$. Here, we do not remark the notations in these equations, because we intend only to show the equivalence in the formulations.

We here extend the irrationality experienced in the quasi-periodic system to designing a new undulator instead of the conventional ones with periodic arrays of magnets. We do not necessarily give a complete expression of the properties of radiation from undulators. It will be developed in a separate paper.

2. Creation of a Qausi-Periodic Lattice

It is known that a quasi-periodic lattice causes sharp diffraction peaks irrationally spaced from each other in reciprocal space. We here review diffraction properties of the quasi-periodicity.

One of the most intuitive ways for creating quasi-periodic lattices is the projection method in which the lattice points on a higher dimensional periodic lattice are projected onto a lower dimensional general plane inclined with irrational gradients against the periodic lattice axes. This method is readily applied to designing a configuration of the magnetic segments on a undulator and the properties of radiation. We here develop the projection method by starting with a simple square lattice to create a 1D quasi-periodic lattice for the sake of basic comprehension.

In Fig. 1, we illustrate a two-dimensional (2D) regular (square) lattice with a cell parameter of a, in which shaded circles refer to scattering matters, for example, corresponding to atoms, molecules and so on in crystals and scattering centers for electron in time domain on the insertion devices. The circles are positioned at the lattice points (x_i, y_i), which can be represented by integers in unit of a.

To produce a quasi-periodic array of matters, we first draw a window, AA'B'B, inclined with a slope of $\tan\alpha$ against the x axis, where $\tan\alpha$ must be irrational. We here adopt an irrational number, $1/\tau$, for $\tan\alpha$,where τ is

$$s(t) = \left(\frac{[\mathbf{n} \times (\mathbf{n} - \dot{\mathbf{r}}/c) \times \ddot{\mathbf{r}}/c\,]}{(1 - \mathbf{n} \cdot \dot{\mathbf{r}}/c)^2} \right) \exp(-2\pi i f\, \mathbf{n}.\mathbf{r}/c) \quad . \qquad (2b)$$

Time, t, in eq. (2b) is usually known as "the retarded time" or "the emitter time". Replacing dt by $(1/\mathbf{n}.\dot{\mathbf{r}})d(\mathbf{n}.\mathbf{r})$ and $s(t)$ by $s(\mathbf{n}.\mathbf{r})$, we can express the equation as a function of a distance along the lining direction of magnets, $(\mathbf{n}.\mathbf{r})$. Here, we do not remark the notations in these equations, because we intend only to show the equivalence in the formulations.

We here extend the irrationality experienced in the quasi-periodic system to designing a new undulator instead of the conventional ones with periodic arrays of magnets. We do not necessarily give a complete expression of the properties of radiation from undulators. It will be developed in a separate paper.

2. Creation of a Qausi-Periodic Lattice

It is known that a quasi-periodic lattice causes sharp diffraction peaks irrationally spaced from each other in reciprocal space. We here review diffraction properties of the quasi-periodicity.

One of the most intuitive ways for creating quasi-periodic lattices is the projection method in which the lattice points on a higher dimensional periodic lattice are projected onto a lower dimensional general plane inclined with irrational gradients against the periodic lattice axes. This method is readily applied to designing a configuration of the magnetic segments on a undulator and the properties of radiation. We here develop the projection method by starting with a simple square lattice to create a 1D quasi-periodic lattice for the sake of basic comprehension.

In Fig. 1, we illustrate a two-dimensional (2D) regular (square) lattice with a cell parameter of a, in which shaded circles refer to scattering matters, for example, corresponding to atoms, molecules and so on in crystals and scattering centers for electron in time domain on the insertion devices. The circles are positioned at the lattice points (x_i, y_i), which can be represented by integers in unit of a.

To produce a quasi-periodic array of matters, we first draw a window, AA'B'B, inclined with a slope of $\tan\alpha$ against the x axis, where $\tan\alpha$ must be irrational. We here adopt an irrational number, $1/\tau$, for $\tan\alpha$,where τ is

known as the golden mean.and frequently used in case of discussing alloy crystals with the icosahedral or decagonal quasi-periodic lattice;

$$\tau = \frac{\sqrt{5}+1}{2}. \tag{3}$$

We will start with this number to develop our model.

We let the window be spanned with an $a \times a$ square cell indicated by thick lines in Fig. 1, which has a width given by

$$w = a(\sin\alpha + \cos\alpha), \tag{4}$$

$$\sin\alpha = \frac{1}{\sqrt{1+\tau^2}}, \tag{5a}$$

$$\cos\alpha = \frac{\tau}{\sqrt{1+\tau^2}}. \tag{5b}$$

We then project the lattice points (x_i, y_i)'s included within the window onto the inclined axis, AA'. This axis will be referred to as 'R// axis' and its normal as 'R⊥ axis'. The coordinates of the lattice point (x_i, y_i) are related to $(R_i^{//}, R_i^{\perp})$ as

$$\begin{pmatrix} R_i^{//} \\ R_i^{\perp} \end{pmatrix} = \begin{pmatrix} \cos\alpha & \sin\alpha \\ -\sin\alpha & \cos\alpha \end{pmatrix} \begin{pmatrix} x_i \\ y_i \end{pmatrix}. \tag{6}$$

The lattice points in the window satisfy the following inequality;

$$0 \le R^{\perp} < w, \tag{7}$$

or in the xy system

$$x\ \tan\alpha \le y < x\ \tan\alpha + a(1+\tan\alpha), \tag{8a}$$

using $w/\cos\alpha = a(1+\tan\alpha)$, or

$$\left(\frac{1}{\tau}\right)x \le y < \left(\frac{1}{\tau}\right)x + \tau a. \tag{8b}$$

The projected points align with two kinds of inter-site distances,

$$d = a \sin\alpha \ , \tag{9a}$$

$$d' = a \cos\alpha \ , \tag{9b}$$

having a ratio of

$$\frac{d'}{d} = \frac{1}{\tan\alpha} . \tag{9c}$$

This is equal to τ ($\approx$1.618...) in the present case, and the points are never positioned in a periodic fashion.

We next formulate the projecting procedure mentioned above. We express the lattice structure within the window by a function $E(\mathbf{R})$ defined as

$$E(\mathbf{R}) = S(\mathbf{R})V(\mathbf{R}) \ , \tag{10}$$

$$\mathbf{R} = (x, y) \ , \tag{11a}$$

or

$$\mathbf{R} = (R^{//}, R^{\perp}), \tag{11b}$$

where $S(\mathbf{R})$ is the structure factor which represents the 2D regular lattice of N matters (N:a sufficiently large number) being expressed by

$$S(\mathbf{R}) = \sum_{i=1}^{N} \delta(\mathbf{R}\text{-}\mathbf{R}_i) \ , \tag{12}$$

and $V(\mathbf{R})$ the window function defined as

$$V(\mathbf{R}) = \begin{cases} 1, & \text{if } \mathbf{R} \text{ is within the window,} \\ 0, & \text{otherwise,} \end{cases} \tag{13a}$$

or

$$V(R^{//}, R^{\perp}) = \begin{cases} 1, & \text{for } 0 \le R^{\perp} < w, \\ 0, & \text{otherwise.} \end{cases} \tag{13b}$$

$E(\mathbf{R})$ can also be represented in the $(R^{//}, R^{\perp})$ system. The projection of the lattice points onto the $R^{//}$ axis is mathematically expressed as

$$P(R^{//}) = \int_{-\infty}^{\infty} E(R^{//}, R^{\perp}) dR^{\perp}. \qquad (14)$$

This function $P(R^{//})$ represents a quasi-periodic array of matters on the R// axis. The positions of the lattice points and their projected coordinates are listed in Table 1 in unit of the cell parameter, a. Further, the distances between the neighboring points along the R// axis are given in the column of 'Distance to next'. A part of the quasi-periodic lattice is drawn in Fig. 2.

We turn to calculating the Fourier transform of $P(R^{//})$. We know that Fourier transform of a projected function is given by a cross-section of the Fourier transform of the original function before projection. We first Fourier-transform eq. (10) and have

$$E(\mathbf{q}) = S(\mathbf{q}) * V(\mathbf{q}) , \qquad (15)$$

where (*) stands for the convolution operation. $E(\mathbf{q})$, $S(\mathbf{q})$ and $V(\mathbf{q})$ are the Fourier transforms of $E(\mathbf{R})$, $S(\mathbf{R})$ and $V(\mathbf{R})$, respectively. The function $S(\mathbf{q})$ has delta functions at shaded circles in Fig. 3 which reveal the reciprocal lattice, that is,

$$S(\mathbf{q}) = N \sum_{i=-\infty}^{\infty} \delta(\mathbf{q}-\mathbf{q}_i) , \qquad (16)$$

where $\mathbf{q}_i$ is the lattice points and the summation is taken all over the reciprocal lattice. $V(\mathbf{q})$ is depicted by a spike (or streak) running normal to the q// axis irrationally inclined against the h axis. We here quantitatively calculate $V(\mathbf{q})$ as follows; From the definition (13), the Fourier transformation of $V(\mathbf{R})$ is carried out as

$$V(\mathbf{q}) = \int_{-\infty}^{\infty} V(\mathbf{R}) \exp(-2\pi i \mathbf{q}.\mathbf{R}) d\mathbf{R}$$

$$= \int_{0}^{w} \int_{0}^{L} \exp\{-2\pi i (q^{//}R^{//} + q^{\perp}R^{\perp})\} dR^{//} dR^{\perp}$$

$$= \frac{\sin(\pi L q^{//})}{\pi q^{//}} \frac{\sin(\pi w q^{\perp})}{\pi q^{\perp}} \exp(\varphi), \qquad (17)$$

where $\exp(\varphi)$ is a phase factor being meaningless at present. (h, k) and $(q^{//}, q^{\perp})$ are the conjugate coordinates of (x, y) and $(R^{//}, R^{\perp})$, respectively. Using eqs. (3), (4) and (5a and b), we can rewrite eq. (17) as

$$V(q^{//}, q^{\perp}) = \frac{\sin(\pi L q^{//})}{\pi q^{//}} \frac{\sin(1.3764...\pi a q^{\perp})}{\pi q^{\perp}} . \qquad (18)$$

Intensity is represented by a square of eq. (17) or (18), that is,

$$V^2(q^{//}, q^{\perp}) = \frac{\sin^2(\pi L q^{//})}{(\pi q^{//})^2} \frac{\sin^2(1.3764...\pi a q^{\perp})}{(\pi q^{\perp})^2} . \qquad (19)$$

The first factor on the right hand side of eq. (19) determines the thickness of the spikes depending on the limited length of the window, L., along the $R^{//}$ axis The second factor in eq. (19) is evaluated as shown in Fig. 4. The profile along the spike is depicted by a curve decreasing to zero at $|q^{\perp}| = 1/w \approx 0.73/a$ in the present model and therefore the full length of the spikes can be deduced to be $2/w \approx 1.45/a$. This can be approximated by $1.8934\exp\{-(|aq^{\perp}|/0.255)^2/2\}$. Convolution of this function with $S(\mathbf{q})$ [see eq. (15)] means that spikes can be drawn through the lattice points in Fig. 3. Thus, the 2D lattice points included within the region shaded in the figure become meaningful. In Table 2, we list the positions of the lattice points contained in the window represented both in (h, k) and $(q^{//}, q^{\perp})$ systems. The intensity distributed on the $q^{//}$ axis is determined by the second factor on the right hand side of eq. (19) being a function of $|q^{\perp}|$. Fig. 5 shows the intensity distribution along the $q^{//}$ axis.

There is another factor of intensity modulation in actual case. That is, the size of the scattering elements results in a monotonous decrease on the intensity with increasing $q^{//}$. We here ignored this effect in Fig. 5, moreover in Table 2. Provided the scattering matters are arranged in a regular way with the same density, the intensity peaks should appear with the same magnitude of 1.8934... (being indicated by a dotted level-line in Fig. 5) and the same inter-peak distance of $1/w$=0.7265...$(1/a)$.

The shaded band in Fig. 3 includes a few pairs of the reciprocal lattice points related by factor 2 in coordinate, for example, $(h_i, k_i)=(1, 1)(1/a)$ and $(2, 2)(1/a)$, $(2, 1)(1/a)$ and $(4, 2)(1/a)$. This kind of pairing corresponds to a generation of second harmonics in undulator radiation. This will make the undulators useless to some extent. To recover this contradiction, we can narrow the band width in Fig. 3, or widen the window width in real space (in Fig. 1). The column of 'Case of $2w$' in Table 2 indicates the peaks appearing after halving the band width in reciprocal space. This problem will be discussed again in creating a quasi-periodic array of magnets on the undulators.

3. Creation of Quasi-Periodic Array of Magnets on Undulator

We here develop a method for creating a quasi-periodic array of alternate positive and negative matters corresponding to the alternate magnetic field on the basis of the principle mentioned above. Three examples will be developed, through which we can establish a way to devise any other quasi-periodic arrays of magnets.

3.1 Straightforward application to two kinds (+/-) of matters (Type 1)

Expecting an alternate arrangement of positive and negative matters on a line that corresponds to the magnet array on undulator, we provide two kinds of sites with open and full circles in Fig. 6. That is, open circles represent some positive matter and full circles negative one with the same magnitude. A new unit cell is defined to include two sites, an open circle and a full circle, with a cell parameter of a', which is rotated 45 degrees against the xy coordinate system as shown in Fig. 6. That is,

$$a' = a\sqrt{2}. \tag{20}$$

The two kinds of matters are positioned at the lattice points (x_i, y_i)'s satisfying a relation

$$\frac{x_i + y_i}{a} = \begin{cases} \text{even integer,} & \text{for positive contribution,} \\ \text{odd integer,} & \text{for negative contribution.} \end{cases} \tag{21}$$

The shaded band in Fig. 3 includes a few pairs of the reciprocal lattice points related by factor 2 in coordinate, for example, $(h_i, k_i)=(1, 1)(1/a)$ and $(2, 2)(1/a)$, $(2, 1)(1/a)$ and $(4, 2)(1/a)$. This kind of pairing corresponds to a generation of second harmonics in undulator radiation. This will make the undulators useless to some extent. To recover this contradiction, we can narrow the band width in Fig. 3, or widen the window width in real space (in Fig. 1). The column of 'Case of $2w$' in Table 2 indicates the peaks appearing after halving the band width in reciprocal space. This problem will be discussed again in creating a quasi-periodic array of magnets on the undulators.

3. Creation of Quasi-Periodic Array of Magnets on Undulator

We here develop a method for creating a quasi-periodic array of alternate positive and negative matters corresponding to the alternate magnetic field on the basis of the principle mentioned above. Three examples will be developed, through which we can establish a way to devise any other quasi-periodic arrays of magnets.

3.1 Straightforward application to two kinds (+/-) of matters (Type 1)

Expecting an alternate arrangement of positive and negative matters on a line that corresponds to the magnet array on undulator, we provide two kinds of sites with open and full circles in Fig. 6. That is, open circles represent some positive matter and full circles negative one with the same magnitude. A new unit cell is defined to include two sites, an open circle and a full circle, with a cell parameter of a', which is rotated 45 degrees against the xy coordinate system as shown in Fig. 6. That is,

$$a' = a\sqrt{2}. \tag{20}$$

The two kinds of matters are positioned at the lattice points (x_i, y_i)'s satisfying a relation

$$\frac{x_i + y_i}{a} = \begin{cases} \text{even integer,} & \text{for positive contribution,} \\ \text{odd integer,} & \text{for negative contribution.} \end{cases} \tag{21}$$

Here, a is the nearest neighbor distance. All the nearest neighbors around an open circle are entirely full circles and *vice versa*. This is to cause an alternate array of positive and negative magnetic fields along the electron path in the undulator.

We let a window AA'B'B have a width of w given by eq. (4) and be inclined with a slope of $1/\tau$ against the x axis by simply following the previous procedure. This method for creating a quasi-periodic lattice will be referred to as 'Type 1'. We then project the lattice points (x_i, y_i)'s included within the window on the inclined R// axis. All the equations from (3) to (9) can be used in common with the present case.

See Fig. 6. The positive and negative matters are alternately aligned in an aperiodic fashion on the R// axis. This configuration is again illustrated in Fig. 7, and the positions of the 2D lattice points within the window and their projected points are listed in Table 3, indicating a quasi-periodic array of d' and d distances between the points. Further, properties of their contributions are listed in the column of 'Contribution', in which we can see an alternate arrangement of positive and negative contributions. It is compared to the alternate magnetic field (or electron trajectory) in the undulator.

All the equations from (15) to (19) can be applied to this model in the same form. $S(\mathbf{q})$ here is the structure factor for the arrangement of matters defined in Fig. 6 and has amplitude peaks only on the reciprocal lattice points (h_i, k_i)'s of

$$(h_i, k_i) = (n_1, n_2)\left(\frac{1}{a}\right), \quad n_1, n_2 \text{ being half-integers,} \qquad (22)$$

which are plotted by small circles in Fig. 8. The intensity diffracted from the quasi-periodic structure created on the inclined $R//$ axis in real space is realized on the q// axis in the figure. Resultant intensity distribution is shown in Fig. 9 and numerical results are listed in Table 4, where we omitted the two kinds of intensity modulations. One is on the thickness of the spikes depending on the size L along the R// direction, and the other appears on the amplitude of the spikes as a monotonous decrease along the q// direction. The latter effect is entirely ignored in this paper. Provided the (+/-) scattering matters are alternately arranged in a regular manner with the same density, the intensity peaks should happen with the same

magnitude of 1.8934... (being indicated by a dotted level-line in Fig. 9) and the same inter-peak distance of $2/w$=1.453...$(1/a)$.

Here, we must note an appearance of a pair of intensity peaks on the q// axis. That is, we can see in Fig. 9 or Table 4 that there is a first strong peak at q//=0.688...$(1/a)$ (due to the reciprocal lattice points G in Fig. 8) and a relatively strong peak at q//=2.065...$(1/a)$ (due to H) which is three times the q// value of the first peak. This kind of harmonicity has been briefly noted in the elementary model discussed in section 2. This contamination of the third harmonic corresponds to an intersection of the streak from the (1.5, 1.5)(1/a) point and the q// axis, which is marked by a small dotted square in Fig. 8 and is considered to be avoided by

1) widening the window,
2) changing the inclination of the q// axis, or
3) choosing different kinds of 2D lattice.

We will present the first and second methods in next subsections. Before going there, we here shortly explain them.

We know that the length of the spike is inversely proportional to the width of window. If we employ a window spanned by a square $(2a \times 2a)$, instead of the $a \times a$ cell as we used, the reciprocal lattice points must have spikes with half length of the present one and small intensity peaks (including the third harmonic) are to disappear. We can also avoid the rational contamination by choosing another irrational slope for the inclined q// axis in Fig. 8. A line DD' shows an example of another possible slope that generates no peak at the third harmonic position.

3.2 Method of widening the window in 2D real space (Type 2)

We double the width of window as shown in Fig. 10. The cell drawn with a corner at the origin, O, includes 4 lattice sites, and the projected pattern on the R// axis, which is schematically presented in Fig. 11, becomes a little complicated in comparison with the previous case. Numerical values of the coordinates are listed in Table 5.

We can see an interesting feature that pairs of the same (+ or -) contributions are alternately aligned. Fig. 12 reveals the reciprocal lattice, on which the length of the spikes is half in comparison with the previous

model. That is, only the lattice points within the narrower region BB'C'C selectively contribute to the intensity distribution on the q// axis, which are marked by 'A' in the column 'Case of $2w$' in Table 4. This shortening of the spikes suppresses the third harmonic that appeared in the previous case. Fig. 13 is the intensity distribution with peaks irrationally separated.

3.3 Method of changing the inclination angle of the q// axis (Type 3)

If the inclined line, i.e., the q// axis does not intersect the spike elongated from the reciprocal lattice point H in Fig. 14, the third harmonic never appears. The extremity of the spike touches the q// axis, if the point H is distant from the axis by $q_{\mathrm{H}}^{\perp}$ satisfying eq. (19) = 0, i.e.,

$$\frac{\sin(\pi w q_{\mathrm{H}}^{\perp})}{\pi q_{\mathrm{H}}^{\perp}} = 0. \tag{23}$$

Then, we have

$$q_{\mathrm{H}}^{\perp} = \frac{1}{w} = \frac{1}{(\sin\alpha + \cos\alpha)a}. \tag{24}$$

According to the geometry in Fig. 14, we can evaluate the inclination angle, α, as

$$\mathrm{IH} = \left(\frac{3\sqrt{2}}{2}\right) \sin\beta = \left(\frac{3\sqrt{2}}{2}\right) \sin\left(\frac{\pi}{4} - \alpha\right) = \frac{1}{\sin\alpha + \cos\alpha}.$$

This is developed into

$$\cos^2\alpha - \sin^2\alpha = \frac{2}{3},$$

then

$$\alpha = \tan^{-1}\left(\frac{1}{\sqrt{5}}\right), \tag{25a}$$

or

$$\alpha = 24.0948\ldots \text{ (degrees)}. \tag{25b}$$

This inclination generates an irrational number $\sqrt{5}$ and never creates a periodic contamination both on the R// and q// axes (See Figs. 15 and 16). The creation of the R(real)-space distribution is illustrated in Fig. 17. Table 6 lists the coordinates used in the creation procedure, which shows two kinds of nearest neighboring distances of 0.9129... and 0.4082... having a ratio of $\sqrt{5}$. This ratio is 1.38... times larger than τ. Table 7 is for q-space in this case. If the (+/-) scattering matters are alternately arranged in a regular manner with the same density, the intensity peaks should take place with the magnitude of 1.7454...(being indicated by a dotted line in Fig. 16) and the inter-peak distance of $2/w$=1.5139... ($1/a$).

4. Real Array of Magnetic Poles of the Undulator

As an example, we choose Type 3 of the pole-array given in Fig.15. That is, let the bars in the positive side correspond to the positive poles and bars in the negative side to negative poles. We can illustrate the quasi-periodic array of magnets as in Fig. 18b). The notes of d' and d put in the figure indicate the distances between the bars, that is, between the centers of the magnetic poles. In the model, we employed the same magnets of d in length and we insert a spacer of (d'-d) between the two magnetic segments of inter-pole distance of d'. The electrons passing through this kind of undulator equally interfere with the fields of positive and negative poles and return to the original orbital path. This model array of magnets will generate a spectrum analogous with the pattern in Fig. 16. Of course, the q// axis must be taken for the energy axis. The width of the maxima (or energy width) depends on the length of the undulator.

Type 1 is also presented in Fig. 18a) for the sake of comparison.

5. Summary and Discussions

We proposed a very different concept for undulator to suppress the rational higher harmonics. By analogy with the diffraction theory, the quasi-periodic array of magnets on the undulator was understood to have a possibility of suppressing rational higher harmonics.

This inclination generates an irrational number $\sqrt{5}$ and never creates a periodic contamination both on the R// and q// axes (See Figs. 15 and 16). The creation of the R(real)-space distribution is illustrated in Fig. 17. Table 6 lists the coordinates used in the creation procedure, which shows two kinds of nearest neighboring distances of 0.9129... and 0.4082... having a ratio of $\sqrt{5}$. This ratio is 1.38... times larger than τ. Table 7 is for q-space in this case. If the (+/-) scattering matters are alternately arranged in a regular manner with the same density, the intensity peaks should take place with the magnitude of 1.7454...(being indicated by a dotted line in Fig. 16) and the inter-peak distance of $2/w$=1.5139... ($1/a$).

4. Real Array of Magnetic Poles of the Undulator

As an example, we choose Type 3 of the pole-array given in Fig.15. That is, let the bars in the positive side correspond to the positive poles and bars in the negative side to negative poles. We can illustrate the quasi-periodic array of magnets as in Fig. 18b). The notes of d' and d put in the figure indicate the distances between the bars, that is, between the centers of the magnetic poles. In the model, we employed the same magnets of d in length and we insert a spacer of (d'-d) between the two magnetic segments of inter-pole distance of d'. The electrons passing through this kind of undulator equally interfere with the fields of positive and negative poles and return to the original orbital path. This model array of magnets will generate a spectrum analogous with the pattern in Fig. 16. Of course, the q// axis must be taken for the energy axis. The width of the maxima (or energy width) depends on the length of the undulator.

Type 1 is also presented in Fig. 18a) for the sake of comparison.

5. Summary and Discussions

We proposed a very different concept for undulator to suppress the rational higher harmonics. By analogy with the diffraction theory, the quasi-periodic array of magnets on the undulator was understood to have a possibility of suppressing rational higher harmonics.

This inclination generates an irrational number $\sqrt{5}$ and never creates a periodic contamination both on the R// and q// axes (See Figs. 15 and 16). The creation of the R(real)-space distribution is illustrated in Fig. 17. Table 6 lists the coordinates used in the creation procedure, which shows two kinds of nearest neighboring distances of 0.9129... and 0.4082... having a ratio of $\sqrt{5}$. This ratio is 1.38... times larger than τ. Table 7 is for q-space in this case. If the (+/-) scattering matters are alternately arranged in a regular manner with the same density, the intensity peaks should take place with the magnitude of 1.7454...(being indicated by a dotted line in Fig. 16) and the inter-peak distance of $2/w$=1.5139... ($1/a$).

4. Real Array of Magnetic Poles of the Undulator

As an example, we choose Type 3 of the pole-array given in Fig.15. That is, let the bars in the positive side correspond to the positive poles and bars in the negative side to negative poles. We can illustrate the quasi-periodic array of magnets as in Fig. 18b). The notes of d' and d put in the figure indicate the distances between the bars, that is, between the centers of the magnetic poles. In the model, we employed the same magnets of d in length and we insert a spacer of $(d'-d)$ between the two magnetic segments of inter-pole distance of d'. The electrons passing through this kind of undulator equally interfere with the fields of positive and negative poles and return to the original orbital path. This model array of magnets will generate a spectrum analogous with the pattern in Fig. 16. Of course, the q// axis must be taken for the energy axis. The width of the maxima (or energy width) depends on the length of the undulator.

Type 1 is also presented in Fig. 18a) for the sake of comparison.

5. Summary and Discussions

We proposed a very different concept for undulator to suppress the rational higher harmonics. By analogy with the diffraction theory, the quasi-periodic array of magnets on the undulator was understood to have a possibility of suppressing rational higher harmonics.

The conventional size of the magnetic segments is about 30 mm in length along the beam path and the length of the undulator can be 4000 mm in the SPring-8 and the total number of magnets becomes about 70. This indicates the band width of the harmonics can be 1% of the energy for a radiation from single electron. We should design the magnet array so that the energy deviations from the higher order reflections by a crystal monochromator may be larger than 1%. This condition could not be difficult to be achieved in real designing. By employing this kind of undulator, we can avoid the band-filtering with total reflection mirrors and the detuning of the coupling of double crystals.

The spacers inserted among the magnetic segments mentioned in section 4 do not positively contribute to the magnetic field, that is, the power of radiation. To recover this power loss, we are required to seek for optimum conditions to create the quasi-periodicity. We can adopt any periodic lattice, for example, triangular, hexagonal, etc. It is worth while trying those possible models in case of real designing of the undulators. We do not discuss more about them in the present work.

We finally suggest a generalized process for designing an undulator with a quasi-periodic array of magnets;

1) Define a 2D or higher dimensional lattice with two kinds of scattering matters (+/-) arranged in an alternate manner.
2) Fourier-transform the higher dimensional lattice structure and get a reciprocal lattice.
3) Draw a line (one-dimensional) irrationally inclined against the lattice axes in the reciprocal lattice and determine the length of the spikes at the reciprocal lattice points so as to avoid a generation of rational harmonics.
4) If 3) is not successful, return to 1).
5) In the real lattice defined in 1), draw a line conjugate to the line defined in the reciprocal lattice in 3) and determine the width of the window by inversing the length of the spikes.
6) Project the lattice points within the window on the line drawn in 5).
7) Check a possibility of realizing the quasi-periodic pole array in the undulator. If impossible, return to 1).

References

1) Winick, H. (1980). *Synchrotron Radiation Research*, edited by H. Winick and S. Doniach, Chapter 2. Plenum Press, New York.

2) Hofmann, A. (1980). Phys. Reports 64, 253.

3) Krinsky, S., Perlman, M.L. and Watson, R.E. (1983). *Handbook on Synchrotron Radiation*, edited by E.E. Koch. North Holland.

4) Kim, K-J. (1986). Nucl. Instr. Methods in Phys. Res. A246, 67.

5) Popik, V.M. and Vinokurov, N.A., Nucl. (1986). Instr. Methods in Phys. Res. A331, 768.

6) Kramer, P. and Neri, R. (1984). Acta Cryst. A40, 580.

7) Janner, A. (1991). Acta Cryst. A47, 577.

8) Bruijn, N.G.de (1981). Proc. K. Ned. Akad Wet. Ser. A43, 39.

9) Jackson, J.D. (1975). *Classical Electrodynamics* , second ed., p.670. John Wiley & Sons, New York.

Table 1 List of the coordinates in unit of a appearing in creating a quasi-periodic lattice in the case of a primitive square lattice. The inclination of the $q^{//}$ axis, $\tan\alpha$, is $1/\tau$ and the width of window, w, is spanned by a single cell ($a \times a$).

i	x (i) (a)	y (i) (a)	$R^{//}$(i) (a)	$R^{\perp}$(i) (a)	Distance to next (a)
1	0	0	0.0000	0.0000	0.5257
2	0	1	0.5257	0.8507	0.8507
3	1	1	1.3764	0.3249	0.5257
4	1	2	1.9021	1.1756	0.8507
5	2	2	2.7528	0.6498	0.8507
6	3	2	3.6034	0.1241	0.5257
7	3	3	4.1291	0.9748	0.8507
8	4	3	4.9798	0.4490	0.5257
9	4	4	5.5055	1.2997	0.8507
10	5	4	6.3562	0.7739	0.8507
11	6	4	7.2068	0.2482	0.5257
12	6	5	7.7326	1.0989	0.8507
13	7	5	8.5832	0.5731	0.8507
14	8	5	9.4339	0.0474	0.5257
15	8	6	9.9596	0.8981	0.8507
16	9	6	10.8102	0.3723	0.5257
17	9	7	11.3360	1.2230	0.8507
18	10	7	12.1866	0.6972	0.8507
19	11	7	13.0373	0.1715	0.5257
20	11	8	13.5630	1.0222	0.8507

Table 2 Intensity distribution on the $q^{//}$ axis in the case of a primitive square lattice with a window (of w in width) spanned by a single cell in 2D real space lattice. The coordinates are represented in unit of $1/a$. The inclination, $\tan\alpha$, is taken to be $1/\tau$. Column 'Case of $2w$' indicates the intensity peaks appearing in case of the half band width [$|q^{\perp}(i)| < 0.36327...(1/a)$].

i	h (i) ($1/a$)	k (i) ($1/a$)	$q^{//}$(i) ($1/a$)	$q^{\perp}$(i) ($1/a$)	Intensity	Case of $2w$
1	0	0	0.0000	0.0000	1.8934	A
2	1	0	0.8507	-0.5257	0.2135	
3	1	1	1.3764	0.3249	0.9336	A
4	2	1	2.2270	-0.2008	1.4637	A
5	2	2	2.7528	0.6498	0.0254	
6	3	1	3.0777	-0.7265	0.0000	
7	3	2	3.6034	0.1241	1.7194	A
8	4	2	4.4541	-0.4016	0.6110	
9	4	3	4.9798	0.4490	0.4365	
10	5	3	5.8304	-0.0767	1.8260	A
11	6	3	6.6811	-0.6024	0.0730	
12	6	4	7.2068	0.2482	1.2700	A
13	7	4	8.0575	-0.2775	1.1429	A
14	7	5	8.5832	0.5731	0.1169	
15	8	5	9.4339	0.0474	1.8681	A
16	9	5	10.2845	-0.4783	0.3420	
17	9	6	10.8102	0.3723	0.7298	
18	10	6	11.6609	-0.1534	1.6324	A
19	10	7	12.1866	0.6972	0.0033	
20	11	6	12.5115	-0.6791	0.0091	

Table 3 List of the coordinates used in creating a quasi-periodic lattice for Type 1 ($\tan\alpha = 1/\tau$ and a window spanned by an $a \times a$ cell).

i	x(i) (a)	y(i) (a)	$R^{//}$(i) (a)	Contribution	Distance to next (a)
1	0	0	0.0000	1	0.5257
2	0	1	0.5257	-1	0.8507
3	1	1	1.3764	1	0.5257
4	1	2	1.9021	-1	0.8507
5	2	2	2.7528	1	0.8507
6	3	2	3.6034	-1	0.5257
7	3	3	4.1291	1	0.8507
8	4	3	4.9798	-1	0.5257
9	4	4	5.5055	1	0.8507
10	5	4	6.3562	-1	0.8507
11	6	4	7.2068	1	0.5257
12	6	5	7.7326	-1	0.8507
13	7	5	8.5832	1	0.8507
14	8	5	9.4339	-1	0.5257
15	8	6	9.9596	1	0.8507
16	9	6	10.8102	-1	0.5257
17	9	7	11.3360	1	0.8507
18	10	7	12.1866	-1	0.8507
19	11	7	13.0373	1	0.5257
20	11	8	13.5630	-1	0.8507

Table 4 Intensity distribution on the $q^{//}$ axis in the case of a composite square lattice with a $a' \times a'$ unit cell. The inclination is $1/\tau$ and the window, w, is spanned by a square of $a \times a$. Column 'Case of $2w$' indicates the intensity peaks appearing in the case of the half band width [$|q^{\perp}(\mathrm{i})| < 0.36327...(1/a)$] in reciprocal space for Type 2.

i	h(i) ($1/a$)	k(i) ($1/a$)	$q^{//}$(i) ($1/a$)	$q^{\perp}$(i) ($1/a$)	Intensity	Case of $2w$
1	0.5	-0.5	0.1625	-0.6882	0.0058	
2	0.5	0.5	0.6882	0.1625	1.6026	A
3	1.5	0.5	1.5388	-0.3633	0.7678	
4	1.5	1.5	2.0646	0.4874	0.3151	
5	2.5	1.5	2.9152	-0.0384	1.8771	A
6	3.5	1.5	3.7659	-0.5641	0.1329	
7	3.5	2.5	4.2916	0.2866	1.1030	A
8	4.5	2.5	5.1423	-0.2392	1.3084	A
9	4.5	3.5	5.6680	0.6115	0.0617	
10	5.5	3.5	6.5186	0.0858	1.8092	A
11	6.5	3.5	7.3693	-0.4400	0.4679	
12	6.5	4.5	7.8950	0.4107	0.5759	
13	7.5	4.5	8.7457	-0.1151	1.7432	A
14	8.5	4.5	9.5963	-0.6408	0.0324	
15	8.5	5.5	10.1221	0.2099	1.4283	A
16	9.5	5.5	10.9727	-0.3159	0.9735	A
17	9.5	6.5	11.4984	0.5348	0.1926	
18	10.5	6.5	12.3491	0.0091	1.8935	A
19	11.5	6.5	13.1997	-0.5167	0.2356	
20	11.5	7.5	13.7255	0.3340	0.8939	A

Table 5 List of the coordinates in creating a quasi-periodic lattice for Type 2 ($\tan\alpha = 1/\tau$ and a window spanned by $2a \times 2a$ cell).

i	x(i) (a)	y(i) (a)	$R^{//}$(i) (a)	Contribution	Distance to next (a)
1	-2	-1	-2.2270	-1	0.5257
2	-2	0	-1.7013	1	0.5257
3	-2	1	-1.1756	-1	0.3249
4	-1	0	-0.8507	-1	0.5257
5	-1	1	-0.3249	1	0.3249
6	0	0	0.0000	1	0.2008
7	-1	2	0.2008	-1	0.3249
8	0	1	0.5257	-1	0.5257
9	0	2	1.0515	1	0.3249
10	1	1	1.3764	1	0.2008
11	0	3	1.5772	-1	0.3249
12	1	2	1.9021	-1	0.5257
13	1	3	2.4278	1	0.3249
14	2	2	2.7528	1	0.5257
15	2	3	3.2785	-1	0.3249
16	3	2	3.6034	-1	0.2008
17	2	4	3.8042	1	0.3249
18	3	3	4.1291	1	0.5257
19	3	4	4.6549	-1	0.3249
20	4	3	4.9798	-1	0.2008

Table 6 List of the coordinates used in creating a quasi-periodic lattice for Type 3 ($\tan\alpha = 1/\sqrt{5}$ and a window spanned by a $a \times a$ cell.)

i	x(i) (a)	y(i) (a)	$R^{//}$(i) (a)	Contribution	Distance to next (a)
1	0	0	0.0000	1	0.4082
2	0	1	0.4082	-1	0.9129
3	1	1	1.3211	1	0.9129
4	2	1	2.2340	-1	0.4082
5	2	2	2.6422	1	0.9129
6	3	2	3.5551	-1	0.9129
7	4	2	4.4680	1	0.4082
8	4	3	4.8762	-1	0.9129
9	5	3	5.7891	1	0.9129
10	6	3	6.7020	-1	0.4082
11	6	4	7.1102	1	0.9129
12	7	4	8.0231	-1	0.9129
13	8	4	8.9360	1	0.4082
14	8	5	9.3442	-1	0.9129
15	9	5	10.2571	1	0.9129
16	10	5	11.1700	-1	0.9129
17	11	5	12.0828	1	0.4082
18	11	6	12.4911	-1	0.9129
19	12	6	13.4039	1	0.9129
20	13	6	14.3168	-1	0.4082

Table 7 Intensity distribution on the $q^{//}$ axis for Type 3 (window spanned by a $a \times a$ cell). Coordinates used for creating the hk space lattice are also listed.

i	h(i) (1/a)	k(i) (1/a)	$q^{//}$(i) (1/a)	$q^{\perp}$(i) (1/a)	Intensity
1	0.5	-0.5	0.2523	-0.6606	0.035
2	0.5	0.5	0.6606	0.2523	1.194
3	1.5	0.5	1.5734	-0.1559	1.515
4	2.5	0.5	2.4863	-0.5642	0.164
5	2.5	1.5	2.8945	0.3487	0.821
6	3.5	1.5	3.8074	-0.0596	1.710
7	4.5	1.5	4.7203	-0.4678	0.402
8	4.5	2.5	5.1285	0.4451	0.473
9	5.5	2.5	6.0414	0.0368	1.732
10	6.5	2.5	6.9543	-0.3714	0.734
11	6.5	3.5	7.3625	0.5414	0.210
12	7.5	3.5	8.2754	0.1332	1.575
13	8.5	3.5	9.1883	-0.2751	1.107
14	8.5	4.5	9.5965	0.6378	0.056
15	9.5	3.5	10.1011	-0.6833	0.020
16	9.5	4.5	10.5094	0.2296	1.277
17	10.5	4.5	11.4223	-0.1787	1.448
18	10.5	5.5	11.8305	0.7342	0.002
19	11.5	4.6	12.3596	-0.5322	0.231
20	11.5	5.5	12.7434	0.3259	0.909

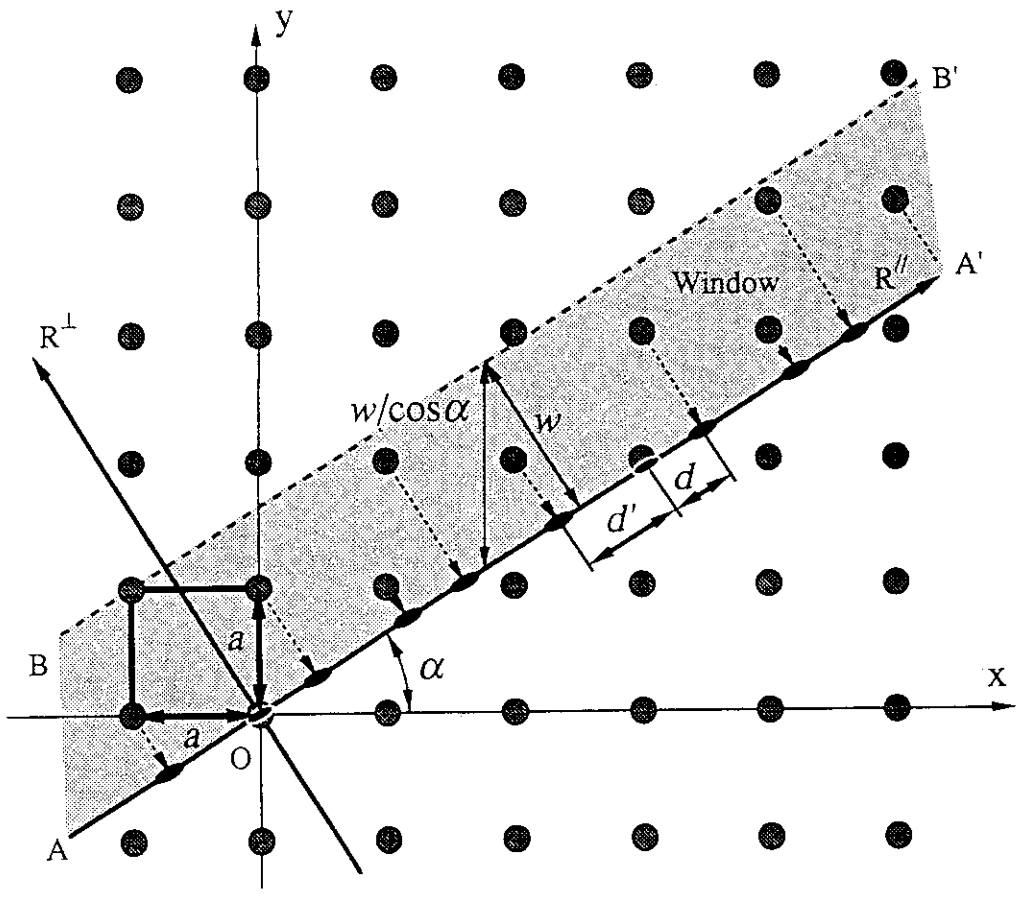

Fig. 1 Creation of one-dimensional quasi-periodic lattice from a 2D square lattice. Lattice points in the window AA'B'B are projected onto the AA' line. As the slope of the line, $\tan\alpha$ is taken to be $1/\tau$, where τ is an irrational number known as the golden mean. Lattice points on the line BB' are excluded. A quasi-periodic lattice is achieved on the AA'.

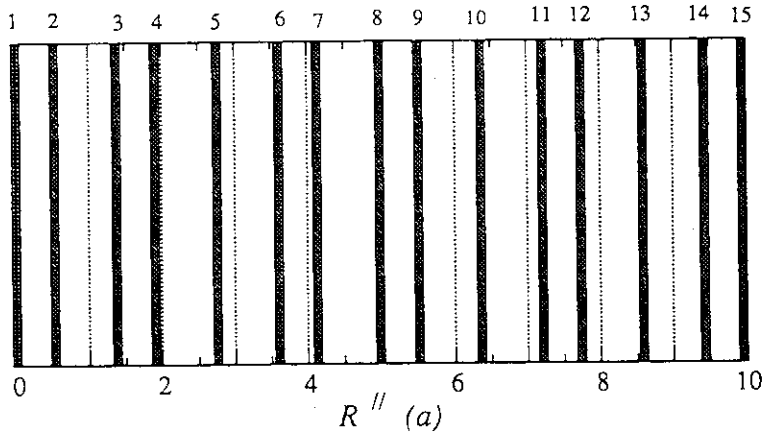

Fig. 2 Quasi-periodic arrangement of matters by bars. d' and d indicate the two kinds of distances between the quasi-lattice points. $d'=\tau d$.

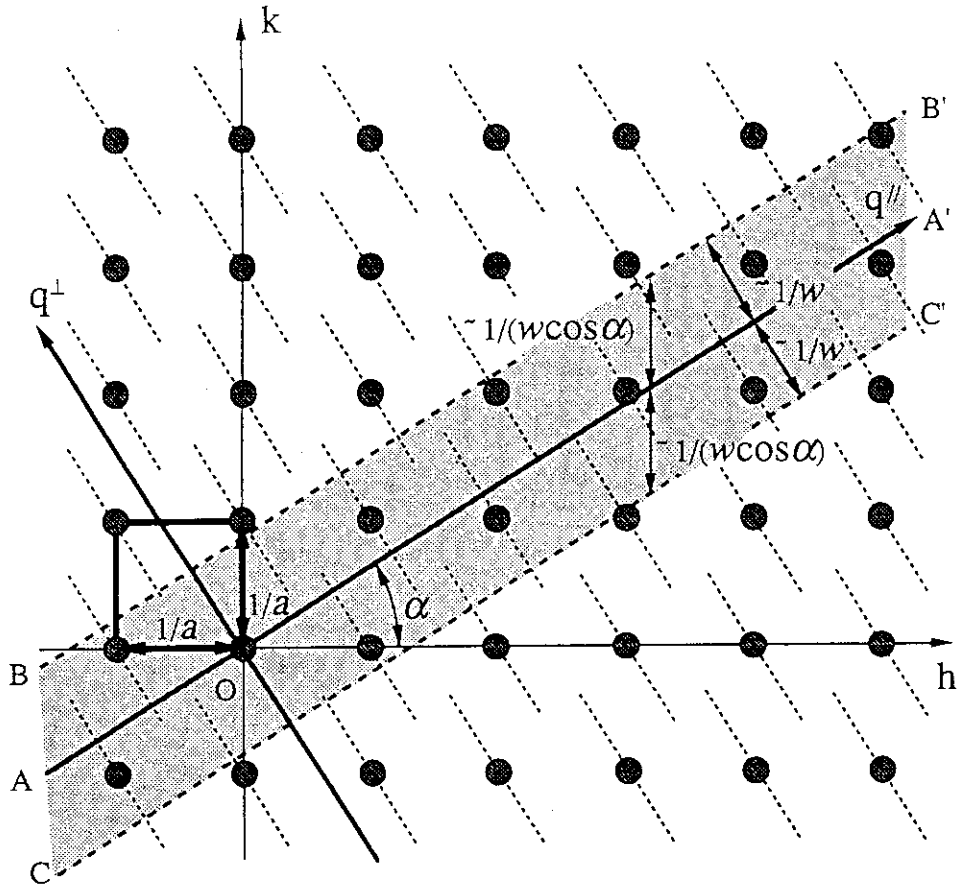

Fig. 3 Fourier transform of the structure given in Fig. 1. Circles reveal the Fourier transform of the two-dimensional regular lattice. Restriction of the lattice points within the window AA'B'B in Fig. 1 causes a spike through the peak positions indicated by small circles. The Fourier transform of the projection is given as a cross-section of the spikes by the inclined q// axis.

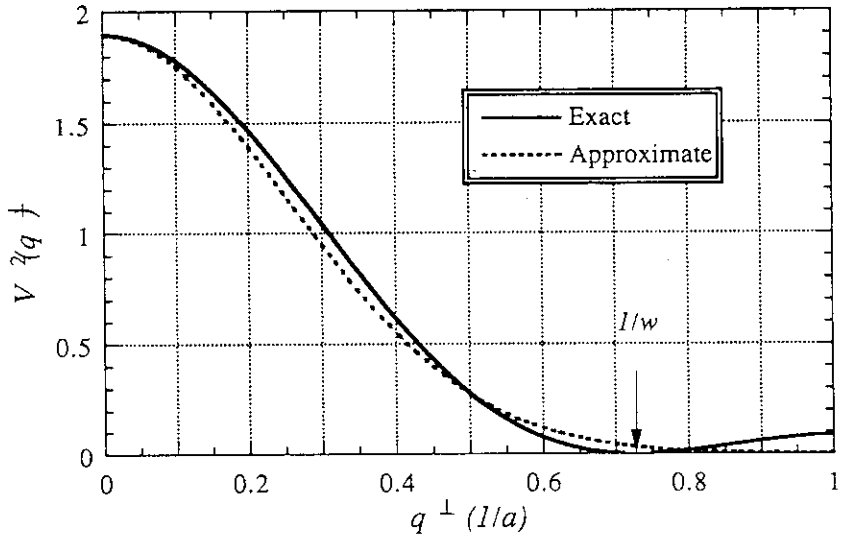

Fig. 4 Type 1:Intensity profile of the spike along the q⊥ direction. The curve behaves sinusoidally. Damping of the profile along the q⊥ direction is very fast and is approximated by a Gaussian function that is drawn in a dotted line.

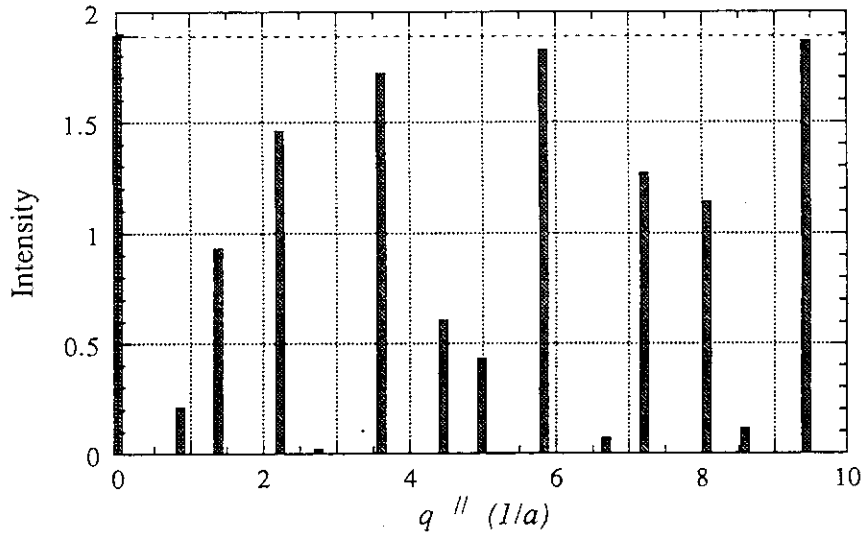

Fig. 5 Distribution of intensity peaks from the quasi-periodic array. The peak positions are dispersed irrationally on the $q^{//}$ axis.

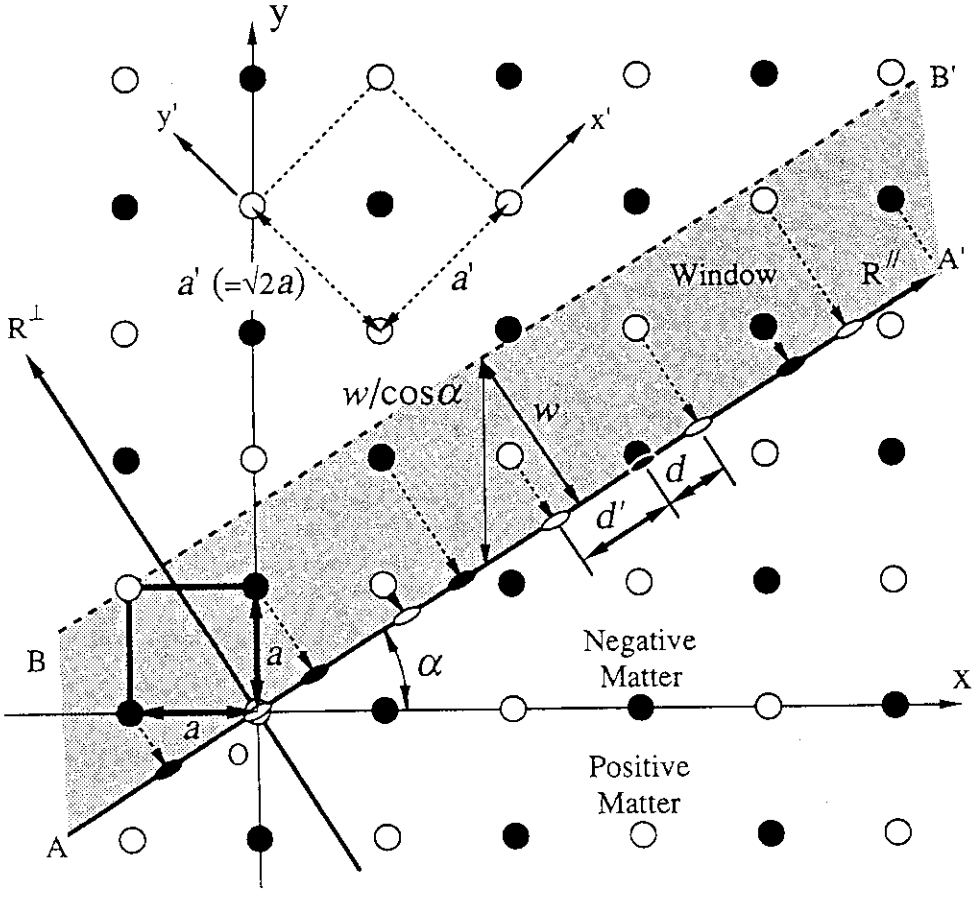

Fig. 6 Type 1 : Creation of one-dimensional quasi-periodic lattice with two kinds of matters from a regular lattice. Open circles represent a positive matter and full circles negative one. Lattice points in the window AA'B'B are projected onto AA'. The slope, $\tan\alpha$, is taken to be $1/\tau$. Lattice points on the line BB' are excluded.

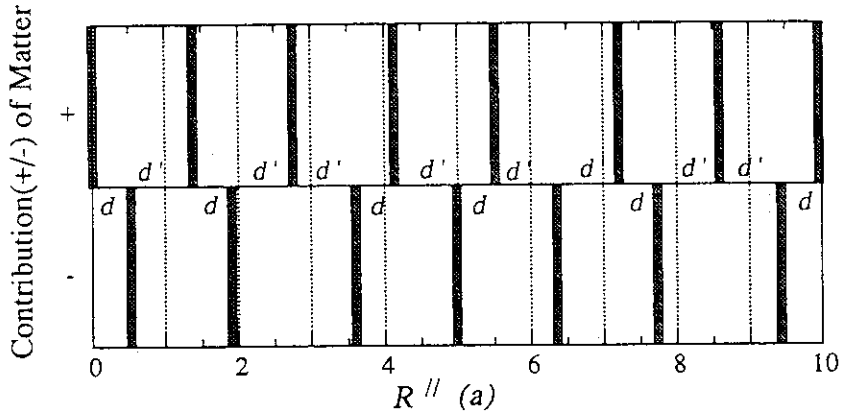

Fig. 7 Type 1 : Quasi-periodic arrangement of +/- matters. Bars represent positive and negative contributions of the matters. d' and d indicate the distances between the quasi-lattice points. $d'=\tau d$.

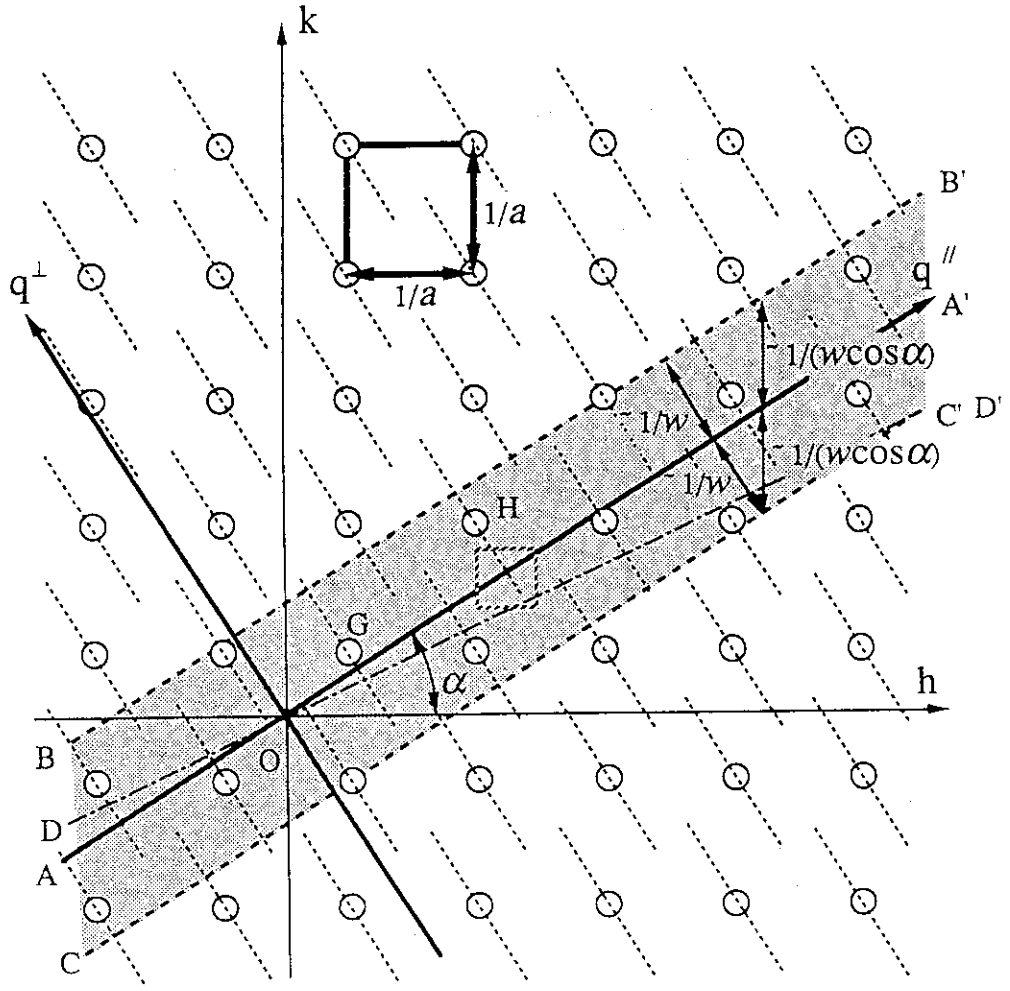

Fig. 8 Type 1 : Fourier transform of the structure given in Fig. 6. Circles reveal the Fourier transform of the two-dimensional regular lattice with positive and negative contributions. The Fourier transform of the projection is given as a cross-section of the spikes by an inclined q// axis.

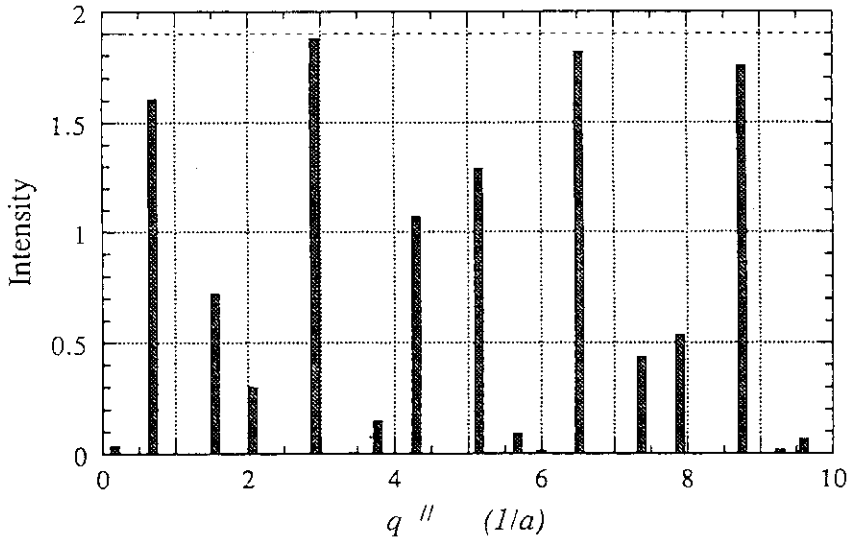

Fig. 9 Type 1 : Intensity distribution from the quasi-periodic array. The peak positions are dispersed irrationally on the q// axis.

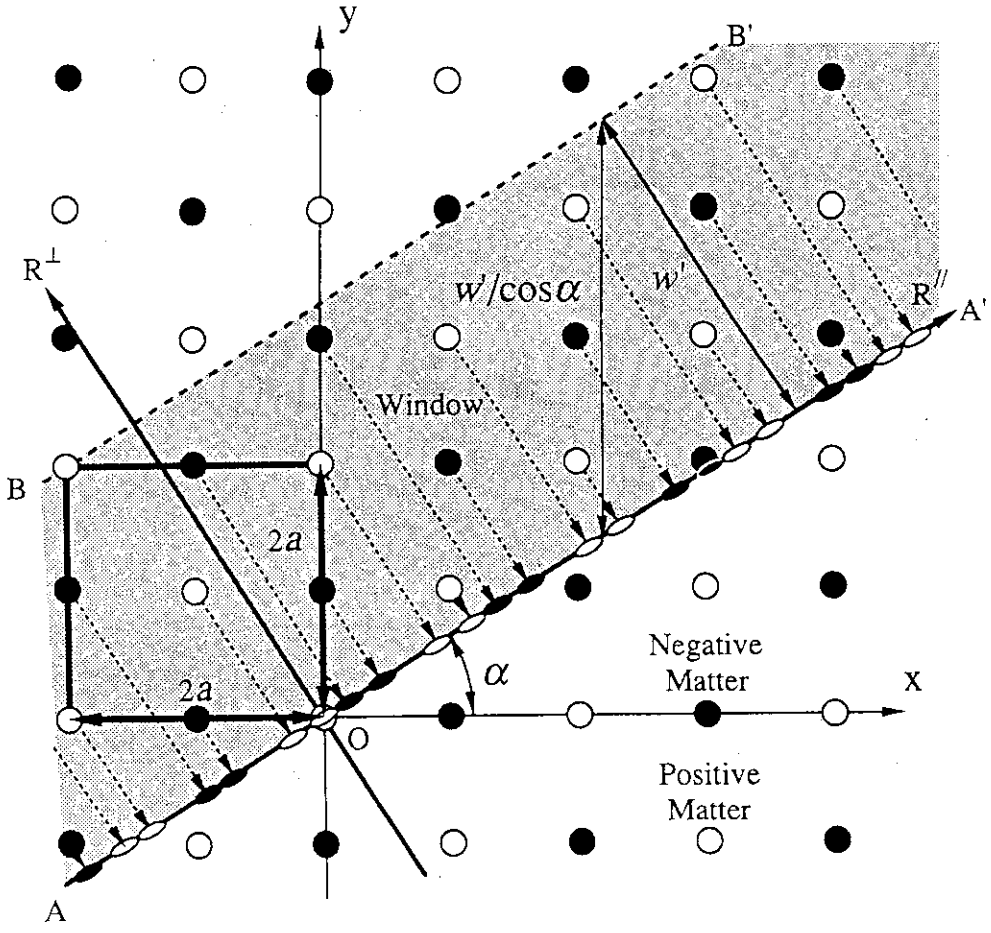

Fig. 10 Type 2 : The width of window, w', is twice that of Type 1. Lattice points in the window AA'B'B are projected onto AA'. The slope of the q// axis, $\tan\alpha$, is taken to be the same $1/\tau$ as in Type 1. A quasi-periodic lattice is created on the AA'.

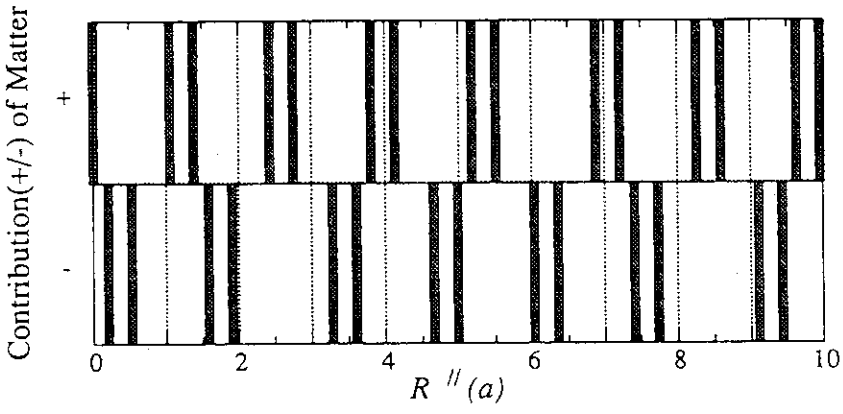

Fig. 11 Type 2 : Quasi-periodic arrangement of +/- matters. A pairing of positive or negative matters is characteristic. There are three kinds of inter-matter distances.

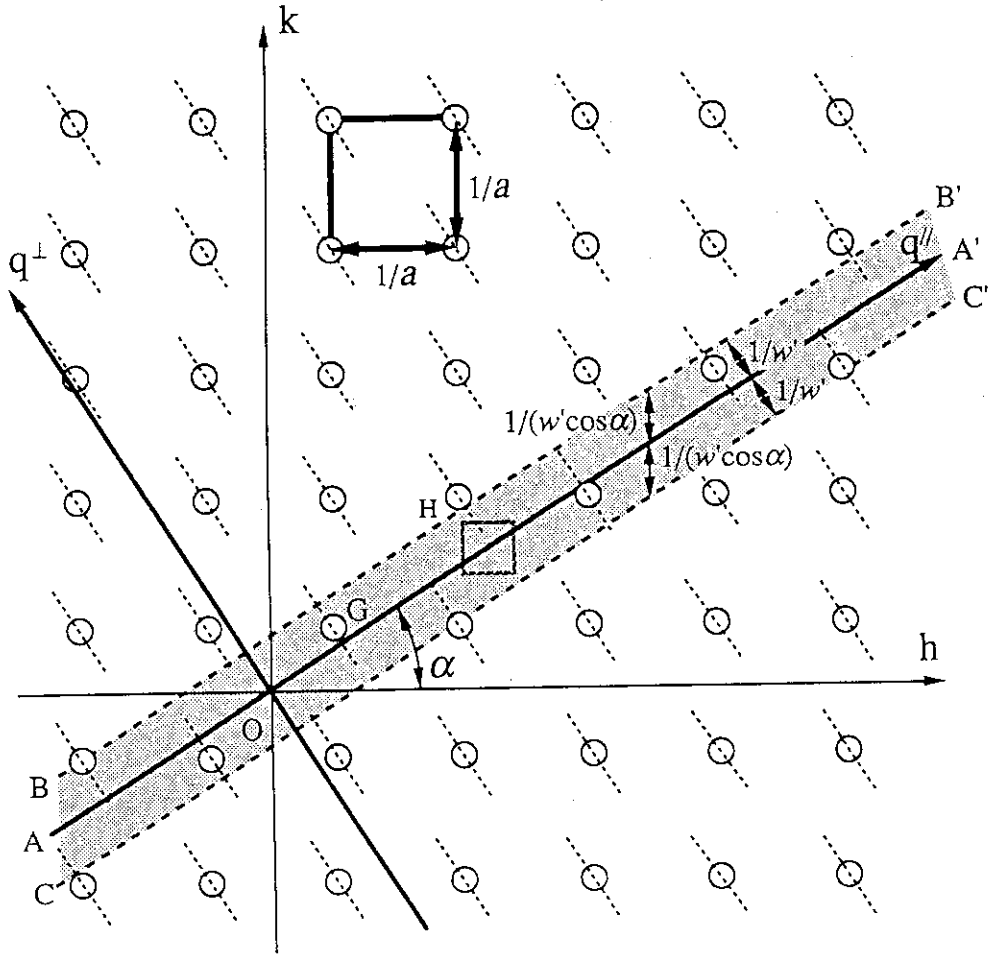

Fig. 12 Type 2 : Fourier transform of the structure given in Fig. 10. Circles revealing the Fourier transform of the two-dimensional regular lattice are the same as in Type 1. Restriction of the lattice points within the wider window AA'B'B of w' in Fig. 10 causes shorter spikes.

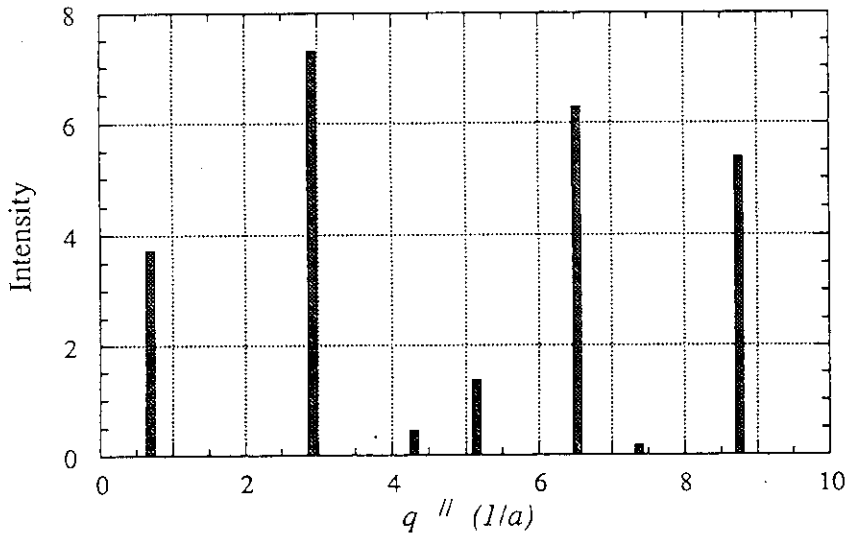

Fig. 13 Type 2 : Intensity Distribution diffracted from the quasi-periodic array of Fig. 11. The peak positions are dispersed irrationally on the $q^{//}$ axis. The density of peaks is less than that in Type 1.

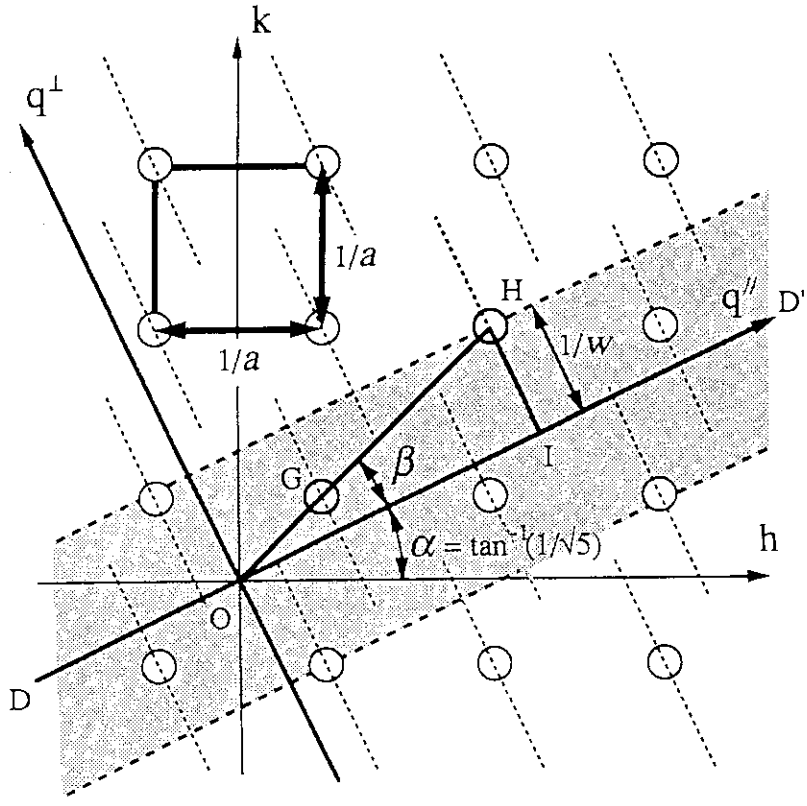

Fig. 14 Type 3 : Geometry to determine an inclination of the $q^{//}$ axis with which a contamination of the third harmonic is suppressed. The circles, G and H, are related in a rational fashion. The point is to avoid a contact of the spike from H and the $q^{//}$ axis. The dotted circle, I, is the extremity of the spike from H. The window in the real space lattice is supposed to include a square of $a \times a$. The cross-section of the spikes does not include any rational contaminations.

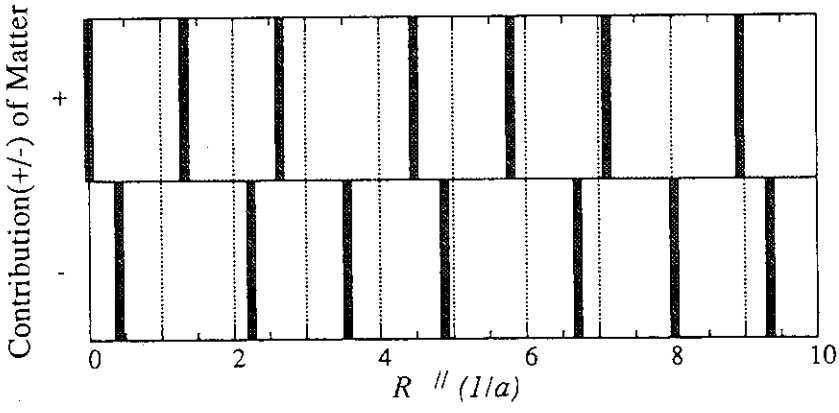

Fig. 15 Type 3 : Arrangement of matters. d' and d are different from those in Type 1, whose ratio is 1.38... times larger.

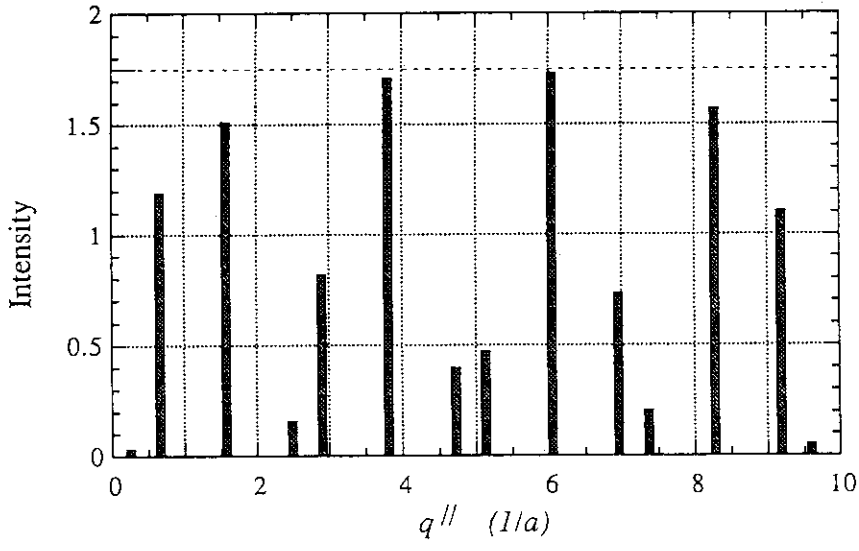

Fig. 16 Type 3 : Intensity distribution given by the geometry in Fig. 15. The peak positions are dispersed irrationally on the q// axis.

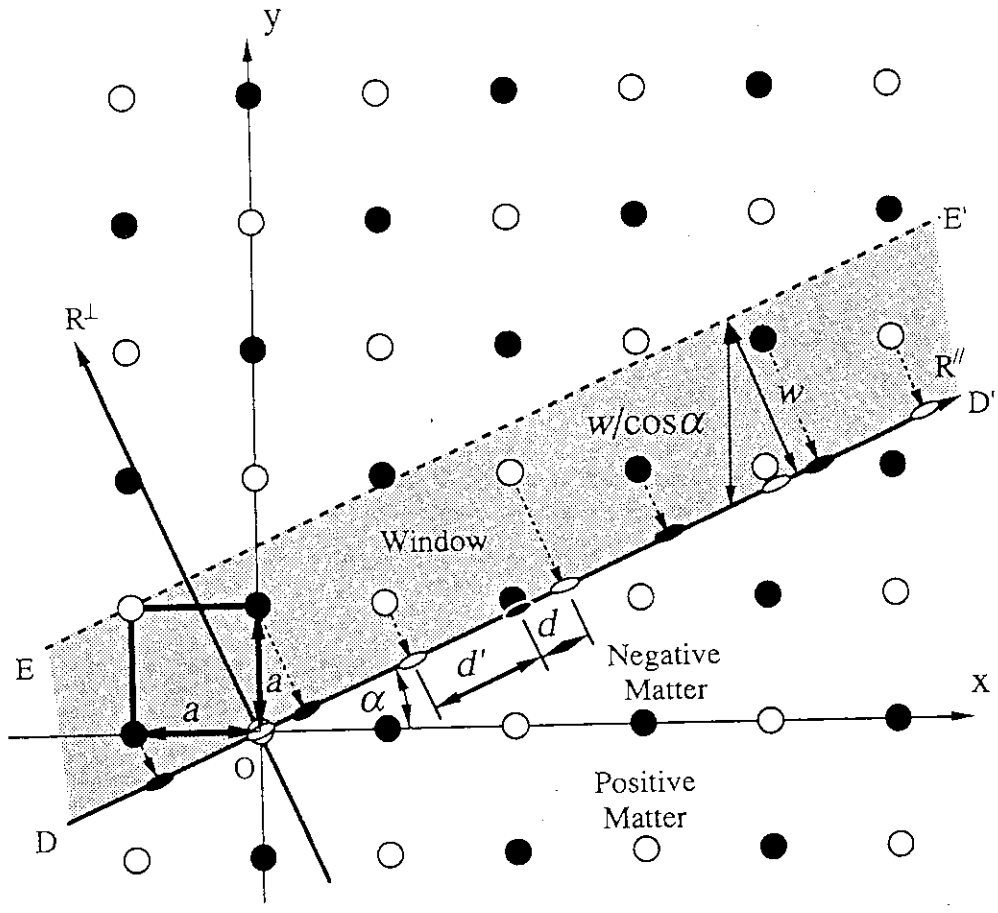

Fig. 17 Type 3 : Real space construction. The slope of the line AA', tanα is $1/\sqrt{5}$. d' and d are different from those of Type 1.

a) Type 1

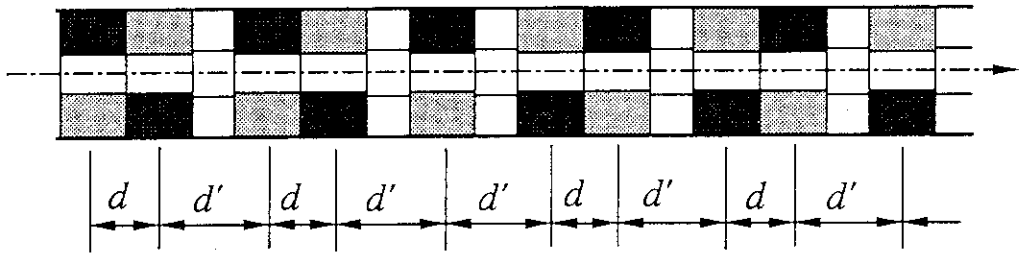

b) Type 3

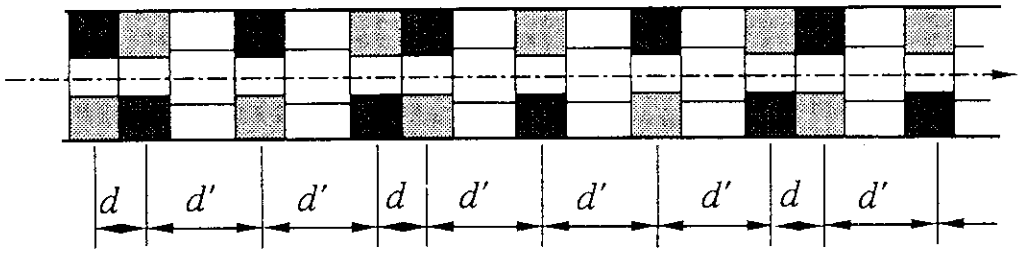

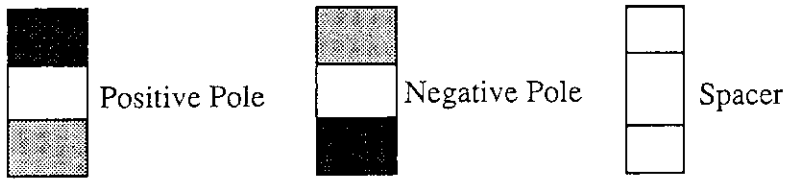

Fig. 18 a) Type 1 : A model structure of magnetic segments on the undulator. This is created by analogy with the structure given in Fig. 6 or Fig. 7. Two kinds of inter-magnet distances are necessary. The distance d is made by the size of the magnet itself and d' the sum of d and a spacer of d/τ. b) Type 3 : This is created by analogy with the structure given in Fig. 15 or Fig. 17. The distance d is made by the size of the magnet itself and d' the sum of d and a spacer of $d(\sqrt{5}\text{-}1)$.